Article

Source and Accumulation Process of Deep-Seated Oil and Gas in the Eastern Belt around the Penyijingxi Sag of the Junggar Basin, NW China

Jiangxiu Qu [1],*[ID], Qinglan Zhang [1], Maoguo Hou [1], Xiujian Ding [1] and Imin Ablimit [2]

[1] School of Geosciences, China University of Petroleum, Qingdao 266580, China
[2] Research Institute of Exploration and Development, Xinjiang Petroleum Administration Bureau, Karamay 834000, China
* Correspondence: 20030040@upc.edu.cn

Abstract: A breakthrough has been made in the recent exploration of the deep oil and gas bearing system in the eastern belt around the Penyijingxi sag of the Junggar Basin. These reservoirs are characterized by mixed sources and multi-stage accumulation. However, this process has not been thoroughly investigated, limiting our understanding of the fundamental rules of hydrocarbon migration and accumulation and making it difficult to determine exploration plans. This study mainly reconstructs this process using biomarkers, carbon isotopes, light hydrocarbons, and fluid inclusions. According to the biomarkers and carbon isotopes for oil-source correlation, Permian crude oil is a mixed-source oil from the Fengcheng Formation (P_1f) and the Xiawuerhe Formation (P_2w) source rocks, while Jurassic crude oil originates from the P_2w source rock. The carbon isotope and light hydrocarbon data demonstrate that Jurassic natural gas has a mixed-gas characteristic with a preponderance of coal-type gas, in contrast to Permian natural gas, which is primarily oil-type gas. The hydrocarbon charging events in the study area were reconstructed based on a comprehensive investigation of the hydrocarbon generation history of source rocks, the homogenization temperature of fluid inclusion, and the burial history of the reservoir. According to the model, the P_1f and P_2w source rocks have made contributions to the current regional oil reservoirs, which provides targets for future exploration.

Keywords: mixed oil; oil-source correlation; hydrocarbon accumulation period; hydrocarbon accumulation process; Penyijingxi sag

1. Introduction

Deep-seated oil and gas exploration has advanced significantly in recent years all over the world, and it is currently the most important area, which will eventually replace conventional oil and gas exploration. The deep-seated source rocks with a high thermal evolution typically undergo multiple stages of hydrocarbon generation and expulsion, facilitating the mixing effect of oil and gas in deep-seated reservoirs. Mixed oils have been discovered in many oilfields around the world, such as the Prudhoe Bay Oilfield in the United States, the Beatrice Oilfield in the United Kingdom, the Persian Gulf Basin crude oil [1,2], the Tarim Basin [3,4], the Junggar Basin [5,6], and the Songliao Basin [7,8] in China. The mixing of biodegraded oil and normal crude oil, as well as low-maturity oil and mature oil, makes it complicated to determine the source and to reconstruct the accumulation process of oil and gas [9–12]. The source determination of the mixed hydrocarbon system has always been challenging; however, previous investigations suggest that a comprehensive analysis based on biomarkers [13,14] and carbon isotopes [15,16] appears to be effective in addressing this problem.

The Junggar Basin is a typical superimposed petroliferous basin in northwest China, with the eastern belt around the Penyijingxi sag (Figure 1) being a current exploration

highlight [17]. The Mobei and Mosuowan oilfields have been found in this area, reflecting great exploration prospects for petroleum [18,19]. Given that there are two sets of source sequences, which have produced hydrocarbons in the study area [20], the discovered hydrocarbons are generally thought to be mixed sourced [10,17] and mainly accumulate in the Permian reservoir in the Mobei nose convex belt and the Jurassic reservoir in the Mosuowan uplift. The source of the hydrocarbons, however, has not been clearly defined, making it difficult to simulate petroleum movement and accumulation [21]. Consequently, the fundamental principles of migration and accumulation of hydrocarbons are not well understood, which restricts exploration strategies.
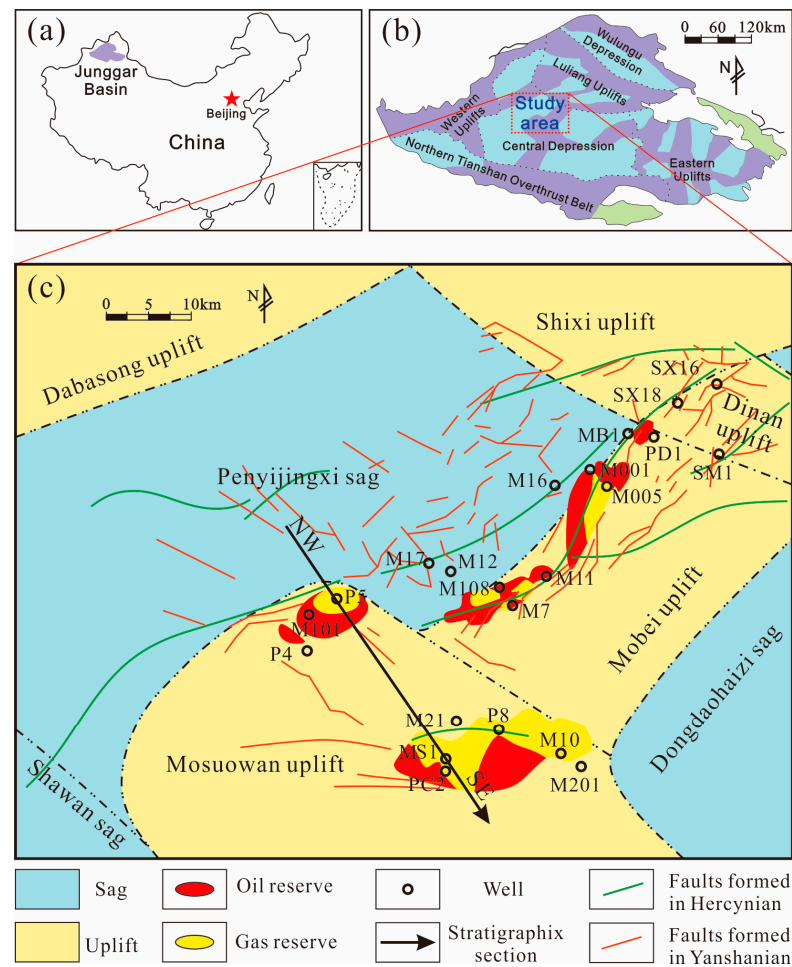

Figure 1. Sketch map showing the locations of the main oil and gas accumulations in the study area. (**a**) The geographic location of the Junggar Basin in China; (**b**) tectonic units in the Junggar Basin (rectangular insert represents the area shown in (**c**)); (**c**) distribution plan of oil and gas in the eastern belt around the Penyijingxi sag. Notes: SX means Shixi, MB means Mobei, PD means Pendong, SM means Shimo, M means Mo, P means Pen, MS means Moshen, PC means Pencan.

Fluid inclusions are generally used for revealing the evolution of geological fluid with the aim to discover the hydrocarbon charging history of a petroliferous basin [22–24]. During the migration and accumulation of hydrocarbon, aqueous fluids are trapped as fluid inclusions in a mineral, which can provide valuable information regarding the chemical as well as physical characteristics related to trapping [25]. Further, hydrocarbon-bearing fluid inclusion compositions can be used for tracing the oil-source signature [26]. In this study, we mainly use biomarkers, carbon isotopes, light hydrocarbons, and fluid inclusions to identify the source and reconstruct the accumulation process of mixed oil in this area. We aim to provide new ideas on the regional characteristics and laws of hydrocarbon enrichment, expand hydrocarbon exploration, and provide references for similar studies.

2. Geological Setting

The Junggar Basin is located in the north of Xinjiang Uygur Autonomous Region in northwest China (Figure 1a). The basin is a triangular shape, with a length of approximately 700 km from east to west and a width of approximately 370 km from north to south. The area is approximately 13.6×10^4 km^2, which is a superimposed basin developed on the Junggar basement in the late Paleozoic and Mesozoic Cenozoic [27,28]. Based on the tectonic location, basement undulation, and regional closure development, the basin can be divided into six main structural units. There are three uplifts (Luliang, Western and Eastern Uplifts), two depressions (Central and Wulungu Depressions), and one piedmont thrust belt (Northern Tianshan Piedmont Thrust Belt) (Figure 1b) [29,30]. The study area is mainly located in the eastern belt around the Penyijingxi sag in the central part of the basin, including the western part of the Dinan uplift, the Mobei uplift, and the central and western regions of the Mosuowan uplift (Figure 1c).

The Junggar Basin has experienced many tectonic movements, such as the Hercynian, Indosinian, Yanshanian, and Himalayan, forming the current tectonic framework [31,32]. The study area is divided by two sets of regional mudstone caps of the lower Cretaceous (including Qingshuihe, Hutubihe, Shengjinkou, and Lianqinmu Formation) and the upper Triassic Baijiantan Formation into three sets of reservoir-seal assemblages, namely the upper, middle, and lower assemblage [33,34]. The lower assemblage is mainly composed of the Permian and Carboniferous reservoirs, while the middle assemblage is mainly composed of the Jurassic reservoir. The sedimentary sequence of the study area includes all strata from the Carboniferous to the Quaternary reservoir. As the research object is the deep reservoirs, it mainly consists of the Carboniferous to Jurassic reservoirs (Figure 2).
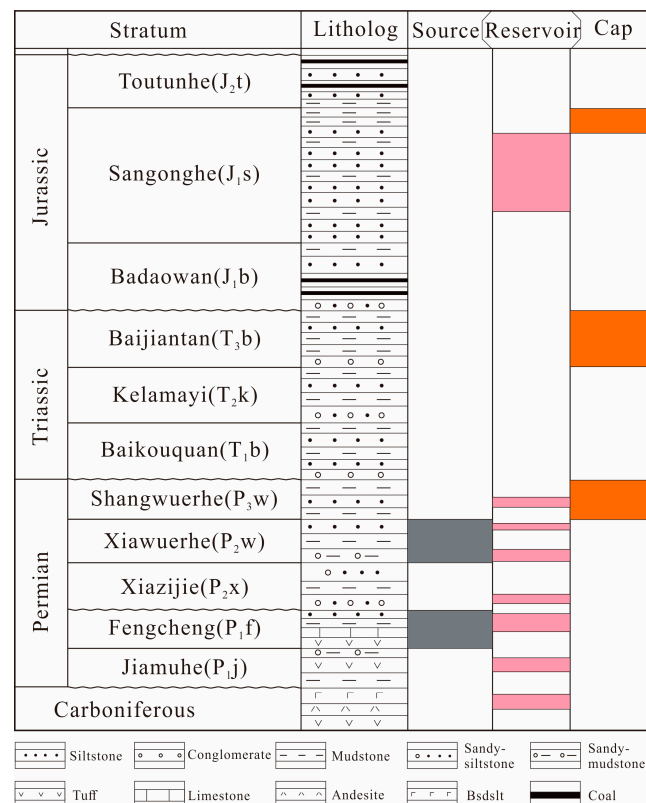

Figure 2. Generalized stratigraphy and source-reservoir-cap-rock combinations in the study area.

3. Analytical Methods

A total of 262 samples were selected for this study, including source rock samples of the P$_1$f and P$_2$w and crude oil samples from the Permian and Jurassic reservoirs. A total of 60 source rock samples were used for total organic carbon (TOC) and Rock-Eval analyses,

and 64 samples were used to measure kerogen elements. A total of 52 source rock samples and 36 crude oil samples were analyzed for specific stable carbon isotope. Sixty source rock samples and twenty-five crude oil samples were used for GC-MS analysis. Twenty natural gas samples were used for light hydrocarbon and carbon isotope of alkanes analyses. Fluid inclusion observation and temperature measurement were carried out on four reservoir rock core samples.

3.1. TOC, Rock-Eval, and Kerogen Element Analyses

TOC and Rock-Eval analyses were used to describe source rock properties. First, the selected samples were crushed to a mesh size of 100. To eliminate carbonate, 6 mol/L HCL was applied to the dried sample powder and allowed to sit for 24 h before TOC testing. The powder should be washed three times with deionized water and dried in an oven. Weigh 200 mg of powder and put it into the capsule, and measure it with the LECO CS-230 analyzer (LECO Corporation, St. Joseph, MI, USA). The device was used to measure free hydrocarbon (S_1) and cracked hydrocarbon (S_2) following the GB/T 18602-2012 [6] standard of the Chinese petroleum industry. The temperature was set at 300 °C and held for 3 min to test S_1 parameters; it was then increased to 650 °C at a rate of 25 °C/min to test S_2 parameters.

The rock samples were crushed into powder (200 mesh) for kerogen element analysis. Hydrochloric and hydrofluoric acids were used to remove inorganic minerals. To remove soluble organic materials, the softened samples were extracted using a Soxhlet extractor and a combination of methylene chloride and methanol (v/v = 9:1). As a result, kerogen was separated from the core sample, and elemental analysis of kerogen was performed using a Vario Micro Cube elemental analyzer (Elementar Analysensysteme GmbH, Hanau, Germany). The carbon and hydrogen contents of kerogen were estimated after oxidizing them to CO_2 and H_2O. At high temperatures, the oxygen was converted into CO, and oxygen concentration was determined.

3.2. Carbon Isotope Analysis

The source rock and oil-bearing sandstone samples were crushed to 80 mesh, and 30 g of the crushed samples was extracted with chloroform for 72 h using the Soxhlet method. The carbon isotopes of the extracts were analyzed using a FLASH HT EA-MAT 253IRMS under the following experimental conditions: the carrier gas was helium (99.999%) at a flow rate of 100 mL/min; the combustion gas was oxygen (99.995%) at a flow rate of 250 mL/min; and the reactor temperature was 980 °C. Chromium oxide, reduced copper, and silver/cobalt oxide were used as reactor filler materials. The results were given in standard per mil notation in relation to the V-PDB standard.

3.3. GC-MS Analysis

Avoid TOC 0.4% (low-quality source rocks) or $S_1 > S_2$ rock sample GC-MS testing to eliminate the potential polluting impacts of external hydrocarbon input. The Agilent 7890GC/5975Ims (Agilent Company, Santa Clara, CA, USA) with an HP-5MS (60 m × 0.25 mm × 0.25 μm) gas chromatography–mass spectrometry was used to analyze the saturated fractions. At a flow rate of 1 mL/min, the carrier gas was helium (99.999%). The initial temperature was 50 °C, which was kept for 1 min before being escalated to 120 °C at a pace of 20 °C/min, and finally to 310 °C at a rate of 3 °C/min. The GC-MS system was set to EI mode, with the current set at 70 eV. The signal abundance of biomarker combinations was at least four orders of magnitude higher in the samples than in the programmed blank samples. As a result, the biomarkers assessed can be regarded as endogenous components, which do not contribute considerable contamination during sample collection and treatment.

3.4. Microthermometry of Fluid Inclusions

Polished thin sections were prepared for fluid inclusion observation in accordance with the Chinese petroleum industry standard SY/T6010-2011 [6], and the results were measured using a Leica DMRXP optical microscope (Leica Corporation, Wetzlar, Germany). A Linkhan THMSG600 heating/freezing system (Linkam Corporation, Redhill, UK) was used to measure microthermometers. There are two steps in fluid inclusion testing. The first step is to study the diagenetic process of hydrocarbon inclusions in thin sections. The homogenization temperature of the aqueous inclusions associated with the oil-bearing inclusions is measured in the second stage. The China Metrology Accreditation (CMA) certified all of the above apparatus and processing techniques. Because of the presence of oil-bearing inclusions, only the homogenization temperature of the initial gas–liquid two-phase aqueous inclusions associated with oil-bearing inclusions was measured. The homogenization temperature of two-phase (liquid and vapor) aqueous inclusions in the samples was tested on a two-sided polished wafer at a heating and cooling rate of 5 °C/min.

3.5. Natural Gas Light Hydrocarbon and Carbon Isotope

The Agilent 6890B GC (gas chromatograph) (Agilent Company, Santa Clara, CA, USA) was used for light hydrocarbon analysis of natural gas. The sample pretreatment and experimental process refer to the oil and natural gas industry standard of the People's Republic of China for stable light component analysis (SY/T 0542-2008 [30]). The instrument was also equipped with a detector of thermal conductivity and flame ionization. In the experiment, the constant temperature furnace was also used to heat the sample. High-purity (99.999%) helium was used as the carrier gas with a flow rate of 1 mL/min. The cylinder outlet pressure was controlled at 0.2 MPa and the air flow rate at 80 mL/min with the split ratio controlled at 150:1. Pona chromatographic columns were used in the experiment. The initial temperature of the chromatographic column box was 30 °C (for 15 min), and then, the temperature was raised to 70 °C at a rate of 3 °C/min, and then to 300 °C (for 10 min) at a rate of 3 °C/min.

The stable carbon isotopes of natural gas were analyzed by using a Finnigan MAT-252 mass spectrometer (Finnigan Corporation, Silicon Valley, CA, USA). The initial temperature was set at 35 °C using a GC–C-irm-MS; it was then raised from 35 °C to 80 °C at a rate of 8 °C/min, and then to 250 °C at a rate of 5 °C/min and held for 10 min. Each sample was analyzed three times and averaged, yielding an analytical precision of ± 0.3‰. The results are reported as relative to the Vienna Pee Dee Belemnite (VPDB).

4. Results and Discussion

4.1. Hydrocarbon Generation Potential and Evolution of Source Rock

4.1.1. Hydrocarbon Generation Potential of Source Rock

The abundance of organic matter is an important factor for determining the hydrocarbon generation potential of the source rock. The P_1f source rock yields a minimum, a maximum, and an average TOC value of 0.13%, 4.28%, and 1.02%, respectively. The range of $S_1 + S_2$ is from 0.01 mg/g to 56.73 mg/g, with an average value of 5.07 mg/g. Overall, 30.68% of the samples fell into the category of fair source rocks, while 40.91% were considered to be good source rocks (Figure 3a). The TOC values of P_2w source rock range from 0.27% to 3.88%, with an average of 1.06%. Their $S_1 + S_2$ values range from 0.12 mg/g to 14.67 mg/g, with an average of 1.92 mg/g. Overall, fair source rocks account for 40.54%, while good source rocks constitute 37.84% (Figure 3b). The above results show that two sets of source rocks have a high organic matter abundance.
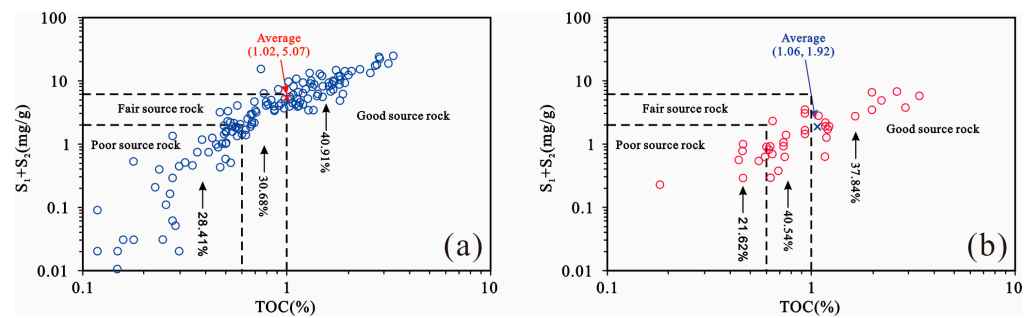
Figure 3. Organic matter abundance of the P_1f (**a**) and P_2w (**b**) source rocks indicated by TOC and Rock Eval $S_1 + S_2$.

The type of organic matter determines the hydrocarbon generation potential of oil-prone or gas-prone source rocks, which is frequently indicated by the kerogen element and rock pyrolysis analyses [35,36]. The hydrogen index (HI) of P_1f source rock has a wide distribution range, from 3.57 to 817.05 mg/g, with an average value of 303.17 mg/g. In the T_{max}–HI relationship diagram, the samples were mainly concentrated within the range of the I–II_1 type. The HI of P_2w source rock ranged from 1.52 to 147.36 mg/g, with an average value of 73.12 mg/g. In the relationship diagram, the samples were mainly concentrated within the range of the II_2–III type (Figure 4a).
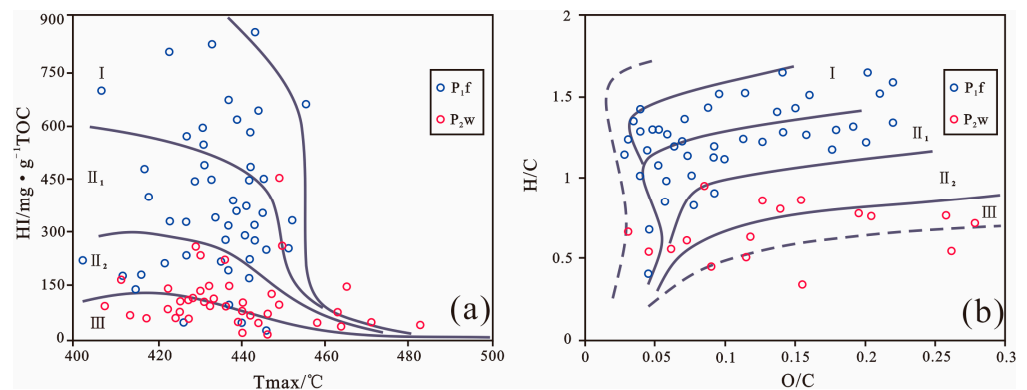

Figure 4. Organic matter type of the P_1f and P_2w source rocks indicated by Tmax and HI (**a**), O/C and H/C (**b**).

The kerogen H/C ratio of the P_1f ranges from 0.27 to 3.23, with an average of 1.40. The kerogen O/C ratio dispersedly distributes in the range of 0.02 to 2.22, with an average of 0.19. The P_2w possesses relatively smaller kerogen H/C ratios, with a range of 0.53 to 1.13 and an average of 0.75. Its kerogen O/C ratio displays a maximum value of 0.76, a minimum value of 0.06, and an average value of 0.33. In summary, the kerogens of P_1f source rock are characterized by types I and II_1, which typify the characteristics of oil-prone rocks. The kerogens of P_2w source rock match well with the characteristics of type III, which are prone to generate gas (Figure 4b). This is consistent with the results obtained through the analysis of rock pyrolysis mentioned above.

4.1.2. Hydrocarbon Generation Evolution of Source Rocks

Reconstruction of the thermal evolution history of hydrocarbon generation in source rocks can be favorable to identify the source and the accumulation stage of hydrocarbon. Based on this geothermal evolution model and stratigraphic burial history, we reconstructed the thermal evolution and hydrocarbon generation process of the source rock in the Penyi-jingxi sag (Figure 5). The results show that at the end of the Early Triassic (250 Ma), the P_1f source rock began to enter the oil generation stage; the peak of oil generation was reached in the Middle Triassic (230 Ma); and the source rock entered the gas generation stage at the end of the Jurassic (150 Ma) and reached the gas generation peak in the Early Cretaceous

(120 Ma). Afterward, its hydrocarbon generation potential gradually declined and was completely lost after the Paleogene. The P_2w source rock reached the peak of oil generation in the Early Cretaceous (130 Ma). In the Early Paleogene, the source rock was highly mature and began to generate gas. In the Middle Paleogene (20 Ma), it entered a peak of gas generation, and it is still in the stage of large amount of gas generation nowadays. This is highly similar to previous studies on the thermal evolution history of source rocks in the study area [37], indicating that the result is viable.
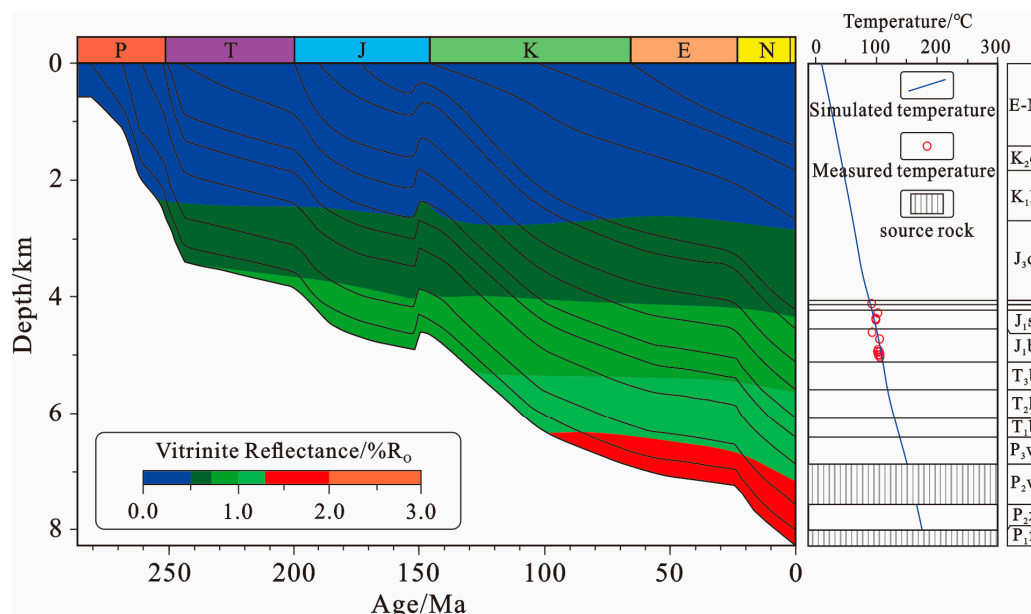

Figure 5. Burial and thermal evolution history of the P_1f and P_2w source rocks.

4.2. Oil and Gas Source Correlation

4.2.1. Organic Matter Source and Sedimentary Environment of Source Rock

The organic matter source of the source rock is controlled by paleoproductivity, while the sedimentary environment affects the preservation of organic matter. Different types of source rock are often formed by different types of organic matter input and preservation environments. The related research is the basis for oil-source correlation. Pr/nC_{17} and Ph/nC_{18} are usually used to evaluate the sedimentary environment of organic matter. In the chart of Pr/nC_{17} and Ph/nC_{18} proposed by Shanmugan [38], most samples of P_1f source rock are distributed in the blue area of the algae-organic matter type, and a few samples fall into the white mixed type area, indicating that P_1f formed mainly in a reducing environment. The P_2w source rock samples are widely distributed in three areas, including the green area of the terrigenous-organic matter type, white area of the mixed type, and blue area of the algae type, generally indicating a sedimentary environment of weak oxidation to weak reduction (Figure 6a).

Sterane compounds can reflect the input of organic matter. The ternary diagram of the relative content of C_{27}, C_{28}, and C_{29} regular steranes is often used to determine the relationship between organic matter sources and crude oil. It is generally believed that the content of C_{29} regular steranes in terrigenous plants is at high levels, with relatively low levels of C_{27} and C_{28}, while C_{27} regular steranes dominate in aquatic organic matter, with relatively low levels of C_{28} and C_{29} [39,40]. The relative content of C_{29} regular steranes of P_1f source rock is slightly higher than that of C_{28} and C_{27}, indicating that the organic matter is mainly input by terrigenous plants and aquatic organic matter. Compared with P_1f source rock, the P_2w has higher content of C_{29} regular sterane, indicating that organic matter has more contributions from terrigenous plants (Figure 6b).
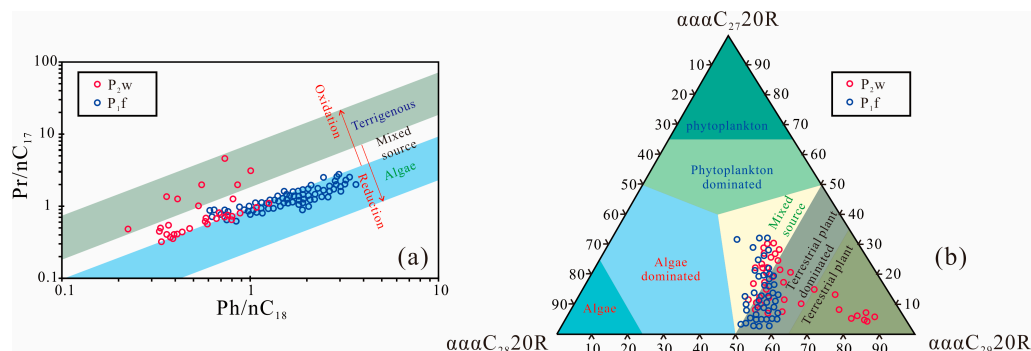
Figure 6. Cross-plot of Ph/nC_{18}-Pr/nC_{17} (**a**) and regular sterane distribution triangle diagram (**b**) of P_1f and P_2w source rocks.

The Pr/Ph is commonly indicative of depositional environments of organic matter and can thus identify the source of crude oil [41,42]. Gammacerane is generally considered as the salinity indicator of sedimentary environments [43,44]. The Pr/Ph and $Gam/C_{30}H$ (Gammacerane/C_{30}Hopane) of P_1f and P_2w source rocks are significantly different. The $Gam/C_{30}H$ of the P_1f is significantly higher than that of the P_2w, while the Pr/Ph of the P_1f is lower than that of the P_2w. In total, 79% of the P_1f sample indicates high $Gam/C_{30}H$ and low Pr/Ph, while 82% of the P_2w sample indicates low $Gam/C_{30}H$ and high Pr/Ph (Figure 7a).
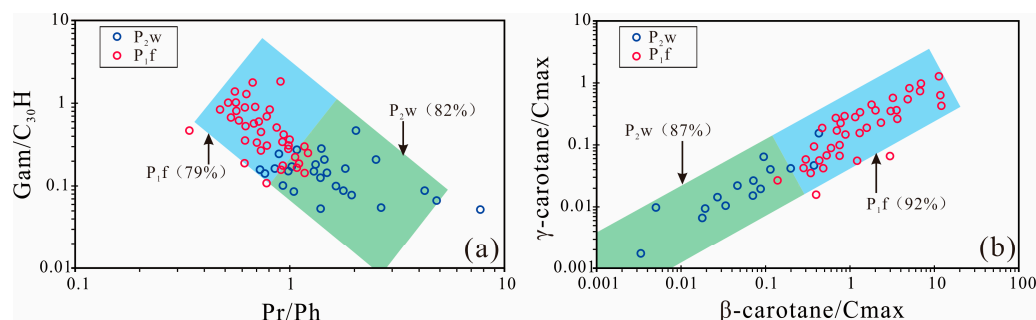
Figure 7. Relationship between Ph/Ph-$Gam/C_{30}H$ (**a**) and β-Carotane/Cmax-γ-Carotane/Cmax (**b**) of P_1f and P_2w source rocks.

β-Carotane is mainly derived from algal organic matter in the sedimentary environment of anoxic and salt lakes [45]. β-Carotane developed widely in the research area, but there are significant differences in its content. The β-Carotane/C_{max} (C_{max} denotes the main peak of n-alkanes) of the P_1f source rock was significantly higher than that of the P_2w. The β-Carotane/C_{max} of P_1f source rock is generally greater than 0.2, while that of the P_2w is generally less than 0.2. Overall, 92% of P_1f source rock samples have the characteristics of high β-Carotane/C_{max} and high γ-Carotane/C_{max}, while 87% of P_2w source rock samples have the characteristics of low β-Carotane/C_{max} and γ-Carotane/C_{max} (Figure 7b).

4.2.2. Source of Crude Oil

In order to compare the relationship between crude oil and source rock, gas chromatography–mass spectrometry (GC-MS) of the reservoir extracts was also carried out. In the cross-plot of Pr/nC_{17} and Ph/nC_{18}, most crude oil from the Mosuowan uplift was distributed in the white area, indicating a weak oxidation and weak reduction sedimentary environment, which is similar to the sedimentary environment of the P_2w source rock. Most crude oil samples from the Mobei nose convex belt are distributed in the blue area, indicating a reduction sedimentary environment (Figure 8a).
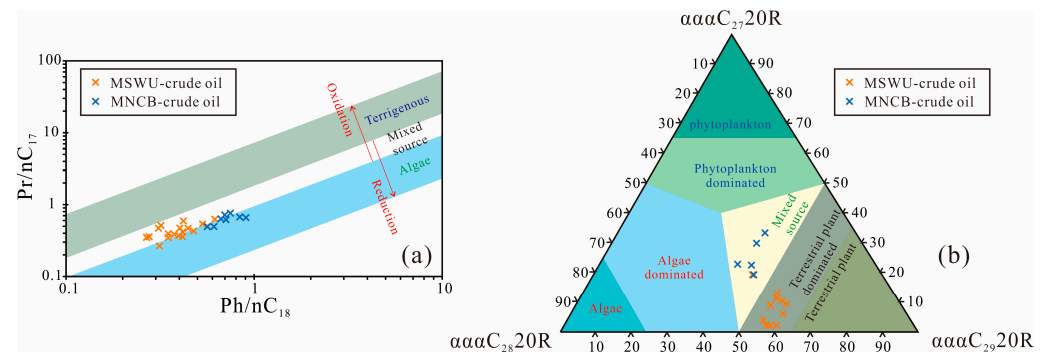
Figure 8. Cross-plot of Ph/nC_{18}-Pr/nC_{17} (**a**) and regular sterane distribution triangle diagram (**b**) of crude oils. Notes: MSWU means Mosuowan uplift, MNCB means Mobei nose convex belt.

In the regular sterane ternary diagram, most crude oil samples from the Mobei nose convex belt are distributed in the area of mixed sources, indicating organic matter from terrigenous and aquatic organisms with mixed-source characteristics. In contrast, crude oil from the Mosuowan uplift has a higher content of C_{29} regular sterane, and most samples indicate that the input of organic matter is mainly terrigenous plant, which is similar to the regular sterane distribution characteristics of the P_2w source rock (Figure 8b).

Mosuowan uplift crude oil is characterized by high Pr/Ph and low $Gam/C_{30}H$. The cross-plots of Pr/Ph and $Gam/C_{30}H$ or β-Carotane/C_{max} and γ-Carotane/C_{max} show that most crude oil samples are distributed in the green area, indicating that Mosuowan uplift crude oil mainly originates from the P_2w source rock. However, compared with the crude oil from the Mosuowan uplift, the crude oil from the Mobei nose convex belt has lower Pr/Ph and higher $Gam/C_{30}H$. In the cross-plot, this crude oil is widely distributed in both green and blue areas, indicating crude oil derived from the source rocks of P_1f and P_2w with characteristics of mixed-source oil (Figure 9).
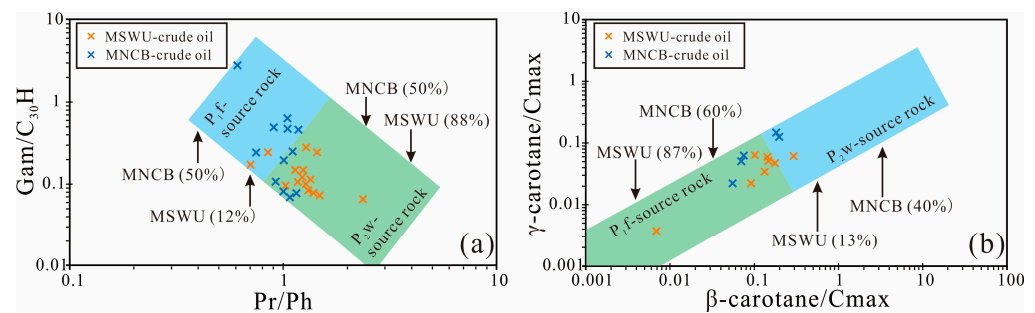

Figure 9. Relationship between Ph/Ph-$Gam/C_{30}H$ (**a**) and β-Carotane/Cmax-γ-Carotane/Cmax (**b**) of crude oils.

Tricyclic terpenes (TTs) are suggested to be derived from primitive algae [46,47]. TTs in marine and salt lake facies crude oil are often dominated by C_{23}, and those in freshwater lake facies crude oil are often dominated by C_{21} [48]. The distribution of TTs is widely used to distinguish oils derived from P_1f and P_2w in the Junggar Basin. The crude oils in the study area can be divided into two types. The first type of crude oil has a higher content of C_{21} and $C_{23}TT$, with a weak ascending-type distribution of C_{20}, C_{21}, and $C_{23}TT$ (Figure 10a,b), indicating crude oil generated in a brackish water environment. This type of crude oil is mainly distributed in the Permian reservoirs of the Mobei nose convex belt. The second type of crude oil, mainly distributed in the Jurassic reservoirs of the Mosuowan uplift, possesses a predominance of $C_{21}TT$ and exhibits a clear mountain peak distribution (Figure 10c), which is possibly derived from a freshwater environment.
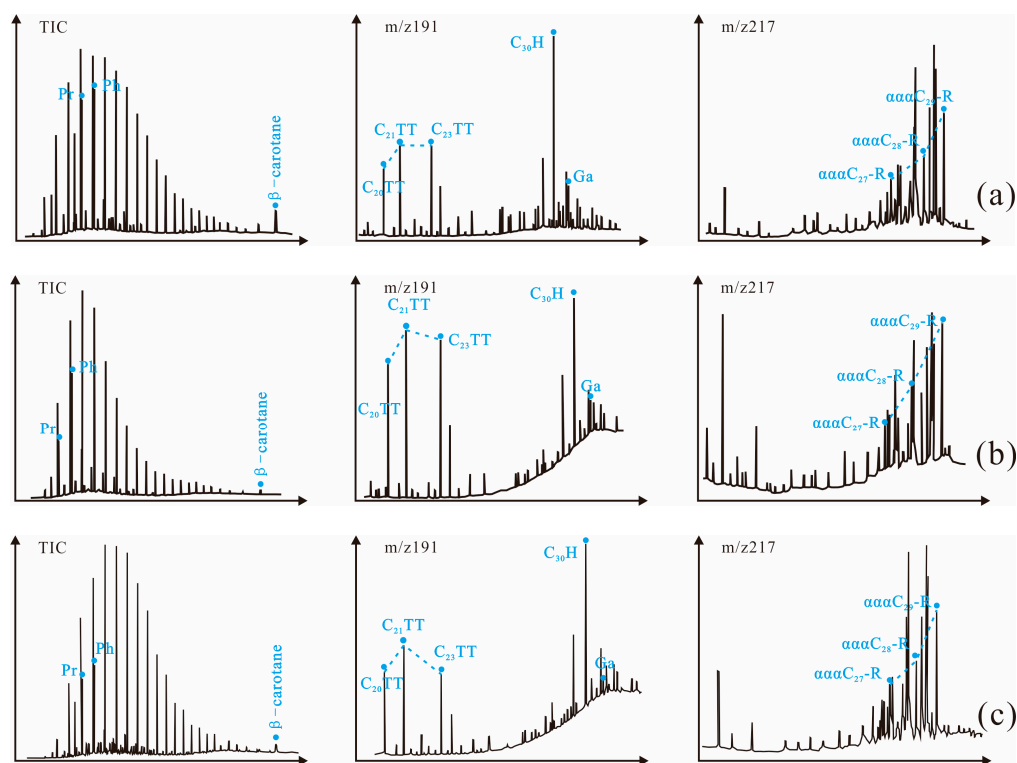
Figure 10. The biomarker characteristics of crude oil in the eastern belt around the Penyijingxi sag ((**a**) SX16-4806.9 m; (**b**) PD1-5267.2 m; (**c**) PC2-5131.9 m).

Based on the distribution characteristics of TTs, the first type of crude oil in the study area is mixed-source oil from the P_1f and P_2w source rocks, while the second type of crude oil originates from the P_2w source rocks.

The carbon isotope records the biological source of organic matter in source rocks, which is frequently used for oil and gas source correlation. The carbon isotope of oil generated through organic matter biologically sourced from terrigenous higher plants is typically heavier than that from aquatic organisms [49]. Carbon isotope analysis of chloroform extracts of P_1f and P_2w source rocks and the Permian and Jurassic crude oil was carried out to show the correlation between source rocks and crude oil. The carbon isotopes of P_1f source rock were the lowest, ranging from −33.01‰ to −27.63‰, with a mean value of −29.75‰, indicating that the P_1f organic matter input is dominated by aquatic organisms. This conclusion is consistent with previous findings suggested by the predominance of green algae or cyanobacteria [50,51]. The carbon isotope values of P_2w are significantly higher than those of P_1f, exhibiting a maximum, a minimum, and an average of −21.21‰, −28‰, and −24.61‰, respectively. This implies a higher input of terrigenous higher plants in P_2w compared to P_1f, which appears to match well with the above findings that the P_2w and P_1f source rocks are characterized by type III and type I or II_1 kerogens, respectively. The carbon isotopes of crude oil from the Permian reservoir in the Mobei nose convex belt range from −29.76‰ to −27.24‰. The crude oil from the Permian reservoir has mixed-source characteristics, with 50% of the samples showing a carbon isotope affinity with P_1f and 50% with P_2w. In addition, the carbon isotopes of crude oil from the Jurassic reservoir in the Mosuowan uplift range from −29.52‰ to −23.89‰, with 86% of the samples indicating crude oil derived from the P_2w source rock (Figure 11). This is consistent with the results of biomarker analysis mentioned above.
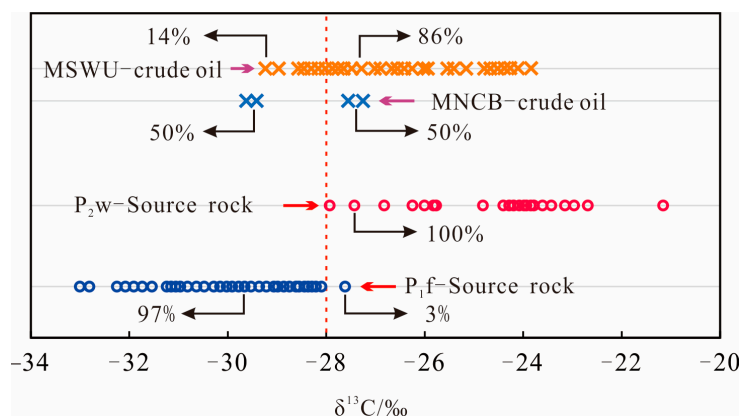
Figure 11. Carbon isotope characteristics of source rocks and crude oil in the study area.

4.2.3. Natural Gas Characteristics and Sources

The $\delta^{13}C_2$ (ethane carbon isotope) of natural gas has a strong inheritance from the original parent material and is less affected by maturity, so it is often used as an indicator to identify the genetic types of natural gas [52]. It is generally believed that the $\delta^{13}C_2$ of coal-type gas is heavier than $-28.0‰$, the $\delta^{13}C_2$ of oil-type gas is basically lighter than $-28.5‰$, and the coexistence zone between $-28.5‰$ and $-28.0‰$ is between coal-type gas and oil-type gas [53]. The $\delta^{13}C_2$ of Permian natural gas samples is significantly lighter than $-28.5‰$, ranging from $-33.6‰$ to $-33.9‰$ for a typical oil-type gas. The $\delta^{13}C_2$ of Jurassic natural gas samples is between $-28.3‰$ and $26.2‰$; most of the $\delta^{13}C_2$ of natural gas samples is heavier than $-28‰$, which belongs to the category of coal-type gas. The $\delta^{13}C_2$ of Permian natural gas is significantly lighter than that of Jurassic natural gas, indicating that it contains more contributions from aquatic organisms. In addition, due to the positive carbon isotope distribution sequence of all natural gas samples, this further indicates that the natural gas in the study area is of organic origin [54,55] (Figure 12a).
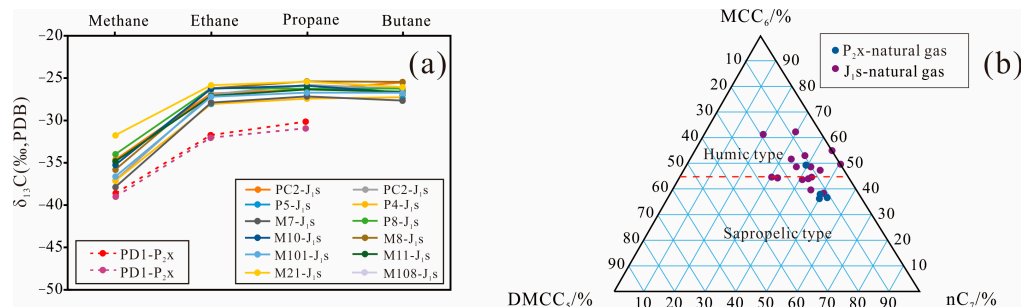

Figure 12. The characteristics of carbon isotope (**a**) and light hydrocarbon (**b**) of Permian and Jurassic natural gas in the eastern belt around the Penyijingxi sag.

Light hydrocarbon is an important component of natural gas, which can reflect the characteristics of natural gas parent material, sedimentary environment, and maturity [56]. C_7 light hydrocarbon compounds are commonly used, including Methylcyclohexane (MCC_6), Dimethylcyclopentane ($DMCC_5$), and normal Heptane (nC_7). The ternary diagram of C_7 light hydrocarbon can reflect the type of natural gas parent material [57]. Among them, due to the MCC_6 being mainly derived from terrigenous plants and having high thermal stability, it is a good indicator of humic organic matter [58]. The majority of Jurassic samples have MCC_6 greater than 45%, while the majority of Permian samples have MCC_6 less than 45%, indicating that Permian natural gas is mainly composed of sapropelic organic matter, while Jurassic natural gas is mainly composed of humic organic matter, which is consistent with the results of carbon isotope (Figure 12b).

4.3. Hydrocarbon Accumulation Process

4.3.1. Fluid Inclusion Characteristics

Hydrocarbons emit fluorescence under ultraviolet light, and their fluorescent colors can reflect the difference in organic component and maturity [59]. The fluorescent color order of organic compounds is brown, yellow, green, and blue-white, which corresponds to the maturity evolution of organic compounds from low to high [60,61]. Multi-stage charging may lead to the coexistence of hydrocarbons with different fluorescent colors [62], which is an effective indicator of the mixing characteristics of hydrocarbons [63,64]. According to the petrographic and fluorescent characteristics of the inclusions, no yellow fluorescent oil inclusions are found in the Permian reservoirs, but a large number of oil inclusions with blue fluorescent and methane gas inclusions without fluorescent display can be seen (Figure 13a,b). Liquid hydrocarbon inclusions mainly occur in feldspar dissolution pores and quartz enlarged edges, while gas inclusions are mainly distributed along the microfractures, which cut through the quartz grains (Figure 13c).
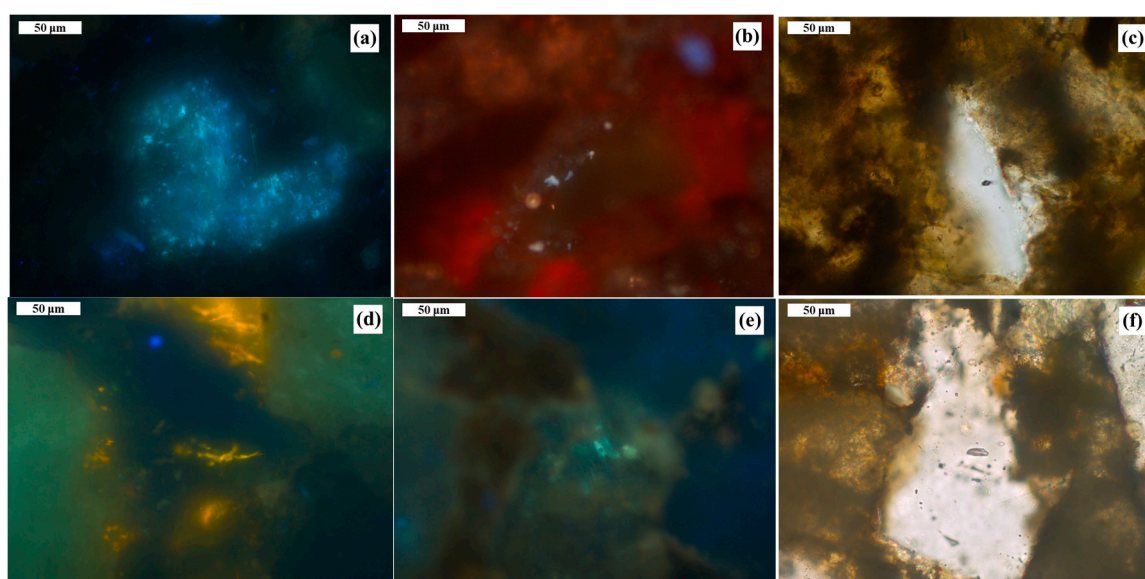

Figure 13. Micrographs of hydrocarbon inclusions in Permian and Jurassic reservoirs in the eastern belt around the Penyijingxi sag. Abbreviations: Transmitted light microphotograph (TLM), UV light microphotograph (ULM). (**a**) Blue fluorescent oil inclusions in the dissolution gap of feldspar particles, well PD1, 5266.59 m, ULM; (**b**) Blue fluorescent oil inclusions in the quartz particle enlarged edge, well PD1, 5266.59 m, ULM; (**c**) Dark-gray gas–hydrocarbon inclusions in the dissolution gap of feldspar particles, well PD2, 5266.59 m, TLM; (**d**) Yellow fluorescent oil inclusions in quartz particle microfractures, well PC2, 5131.95 m, ULM; (**e**) Blue fluorescent oil inclusions in the dissolution gap of feldspar particles, well PC2, 5131.95 m, ULM; (**f**) Dark-gray gas–hydrocarbon inclusions in quartz particle microfractures, well PC2, 5131.95 m, TLM.

Two distinct groups of fluid inclusions were recognized in the Jurassic reservoir. The first group consists of irregularly shaped oil inclusions with yellow fluorescent color, which occur within the quartz particle microfractures (Figure 13d). The second group's fluid inclusions are oil and gas inclusions with blue and non-fluorescent colors, respectively, which are trapped in the microfractures of quartz particles and the dissolution gap of feldspar particles (Figure 13e,f). It is inferred that the oil inclusions in the first group occurred during the charging stage of oil with a relatively low maturity, while the oil and gas inclusions in the second group are the product of the highly mature stage.

The Th (homogenization temperature) of fluid inclusions is an important parameter commonly used in the study of the hydrocarbon accumulation process. It is adjusted by the cold and hot platform. When the multi-phase system in the inclusions becomes homogeneous, the temperature, which reaches the homogenization of the phase state

of the inclusions, is called the Th of fluid inclusions. Compared with the fluctuation of Th of hydrocarbon inclusions, the Th stability of aqueous inclusions is relatively high. Therefore, the Th of aqueous inclusions associated with hydrocarbon inclusions is studied and measured [65,66].

The Th of the Permian reservoir aqueous inclusions in the Mobei nose convex belt is shown in Figures 5–13. A large number of blue fluorescent oil inclusions and gas inclusions are found in this reservoir, but no yellow fluorescent oil inclusions are found. Among them, the Th of the aqueous inclusions associated with the blue fluorescent oil inclusions is between 79 °C and 138 °C, and its peak value is between 80 °C and 90 °C. The Th of the aqueous inclusions associated with the gas inclusions is between 119 °C and 141 °C, and its peak value is between 130 °C and 140 °C. The Th of the Permian reservoir in the Mobei nose convex belt presents a bi-modal feature (Figure 14a); it is considered that the Permian reservoir experienced at least two stages of hydrocarbon charging.
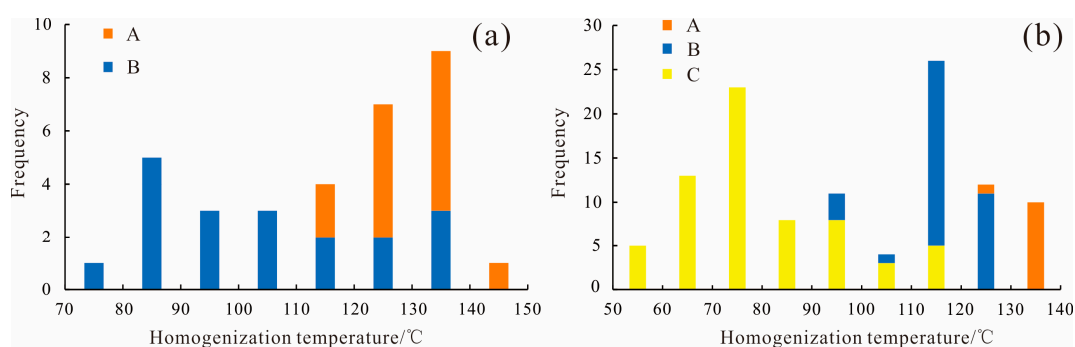

Figure 14. Histogram of Th distribution of aqueous inclusions associated with hydrocarbon inclusions of Permian (**a**) and Jurassic (**b**) reservoirs in the eastern belt around the Penyijingxi sag. A: Aqueous inclusions associated with gas inclusions; B: Aqueous inclusions associated with blue fluorescent oil inclusions; C: Aqueous inclusions associated with yellow fluorescent oil inclusions.

The Th of the aqueous inclusions associated with the yellow fluorescent oil inclusions in the Jurassic reservoir of the Mosuowan uplift is distributed between 50.4 °C and 119.4 °C, and its peak is between 70 °C and 80 °C. The Th of the aqueous inclusions associated with the blue fluorescent oil inclusions is between 90.3 °C and 129 °C, and its peak is between 110 °C and 120 °C. The Th of the aqueous inclusions associated with the gas–hydrocarbon inclusions ranges from 129 °C to 139 °C, with a peak between 130 °C and 140 °C. The Th of the Jurassic reservoir presents a bi-modal feature (Figure 14b); it is considered that the Jurassic reservoir experienced at least two stages of hydrocarbon charging.

4.3.2. Hydrocarbon Charging Period

The depth and corresponding geological age for the formation of fluid inclusions can be determined based on the Th of aqueous inclusions and the reservoir's burial history, further determining the hydrocarbon charging time [67–69]. Two major hydrocarbon charging stages were recognized by the Th and the reservoir's burial history. The first charging stage in the Permian reservoir is the early Jurassic (approximately from 190 Ma to 175 Ma). The second stage is after the late Cretaceous (approximately from 82 Ma to the present) (Figure 15a). It can be seen that the period of hydrocarbon accumulation in the Jurassic reservoir is different from that in the Permian reservoir. The first stage of hydrocarbon charging in the Jurassic reservoir occurred in the early Cretaceous (approximately from 122 Ma to 116 Ma), while the second stage of charging occurred in the late Paleogene to early Neogene (approximately from 35 Ma to 15 Ma) (Figure 15b).
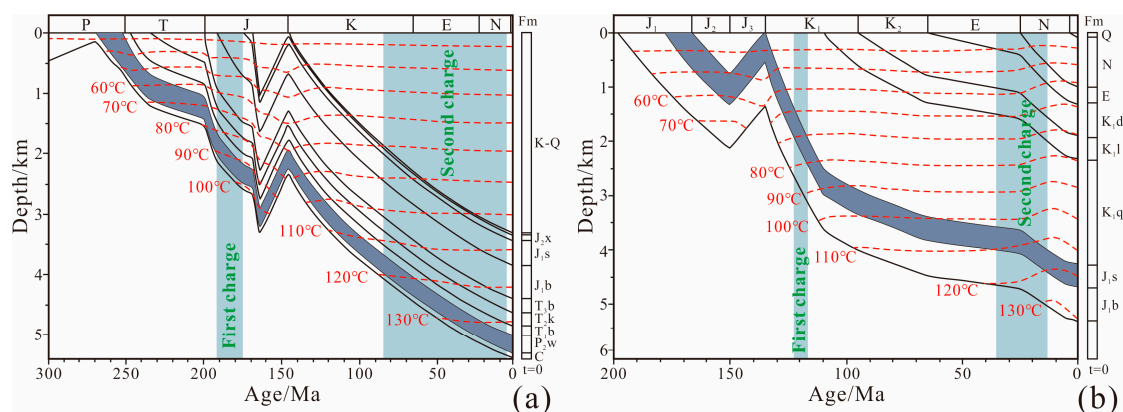
Figure 15. Burial and geothermal history of Permian (**a**) and Jurassic (**b**) reservoirs in the eastern belt around the Penyijingxi sag.

4.3.3. Hydrocarbon Charging Process

Hydrocarbon charging in the Permian reservoir began in the early Jurassic. According to the thermal evolution history of the source rock, in the early Jurassic, the P_1f source rock entered a highly mature evolution stage and began to generate condensation. At this time, the P_2w source rock did not enter a large number of hydrocarbon generation stages. It is believed that the hydrocarbon charged in the early stage of the Permian reservoir was derived from the P_1f source rock, and the blue fluorescent oil inclusions in the reservoir may be the products of this stage of hydrocarbon charging. In addition, no yellow fluorescent oil inclusions were found in the Permian reservoir, reflecting that it could only accumulate highly mature crude oil. The second stage of hydrocarbon charging in the Permian reservoir occurred after the late Cretaceous. At this stage, both the P_1f and P_2w source rocks had entered the gas generation stage, and oil-type gas from the P_1f and coal-type gas from the P_2w were charged into the Permian reservoir. The large amount of gas inclusions discovered in the Permian reservoir may have formed during this stage.

The quantitative fluorescence technology mainly includes quantitative grain fluorescence (QGF), QGF on extract (QGF-E), and total scanning fluorescence (TSF). QGF parameters, such as the QGF index and λmax (maximum wavelength), are commonly used to detect the abundance and maturity of hydrocarbon inclusions in particles to identify paleo-oil layers. The QGF index of the paleo-oil layers is typically greater than 4, while it is less than 4 in the water layers. λmax of the QGF spectrum can indicate the maturity of hydrocarbon: 350 nm < λmax < 400 nm for condensate, 400 nm < λmax < 450 nm for light oil, 450 nm < λmax < 550 nm for moderately heavy oil, λmax > 550 nm for heavy oil [70]. QGF-E is frequently used to detect the relative concentration and maturity of adsorbed hydrocarbons, to identify the current or residual oil layers, and to determine the oil–water interfaces. Generally, the QGF-E intensity of current and residual oil layers is higher than 40 pc, while that of the water layers is lower than 20 pc. When it comes to the λmax of QGF-E, 350 nm < λmax < 400 nm, 420 nm < λmax < 460 nm, and 460 nm < λmax < 500 nm typically indicate condensate, light oil, and heavy oil [71].

The QGF index of the overall reservoir samples in the Jurassic Sangonghe Formation ranges from 2.8 to 4.9. The QGF indices are all less than 4 below 4456 m, and the QGF index is greater than 4 above 4456 m, indicating a depth of 4456 m for the paleo-oil–water interface. The fluorescence spectrum of oil inclusions exhibits a λmax value range of 401.7–426.0 nm, which indicates that the paleo-oil is medium to light oil (Figure 16).
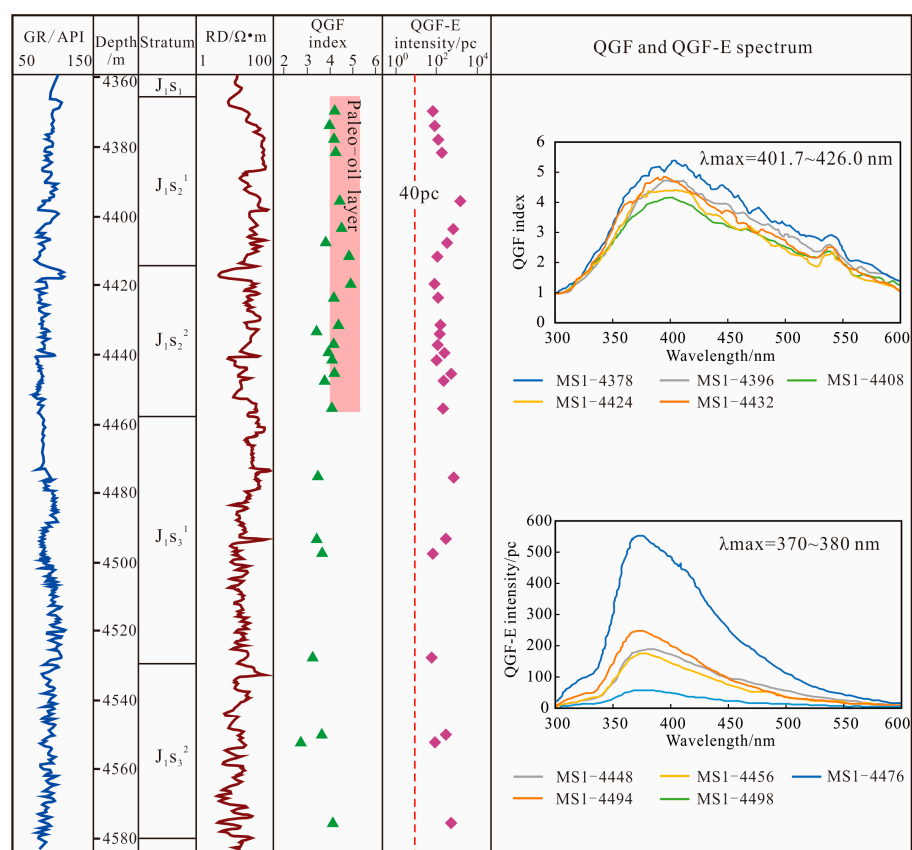
Figure 16. Quantitative fluorescence analysis of samples from Well Moshen1 in the Mosuowan uplift (quantitative fluorescence data from Ref [72]).

The reservoir samples from the Jurassic Sangonghe Formation range in QGF-E intensity from 64.1 pc to 1596.0 pc, with a QGF-E intensity of at least 40 pc for every sample. The λmax of the QGF-E spectrum ranges from 370 nm to 380 nm, indicating that the current hydrocarbons are mainly condensate (Figure 16). This reflects that the Jurassic reservoir is mainly charged with highly mature oil and gas of the second stage, and the charging intensity is much greater than that of the first stage.

The first oil charging time of the Jurassic reservoir occurred in the early Cretaceous, which does not match the peak period of hydrocarbon generation of P_1f and P_2w source rocks. It is hypothesized that the oil and gas from this stage may have been derived from the stratum in the underlying Jurassic reservoir, and the first stage of hydrocarbon accumulation in the Jurassic reservoir may be a secondary oil reservoir. Before the Jurassic reservoir, the P_1f source rock entered a peak period of oil generation, and the oil mainly accumulated in the stratum below the Jurassic reservoir (Figure 17). The early oil reservoir, which was derived from the P_1f source rock, was destroyed by the faults created by the Yanshanian movement in the early Cretaceous. This provided the power for the upward adjustment of the hydrocarbon, which caused the early crude oil gathered in the Carboniferous and Permian reservoirs to move along the fault to the Jurassic reservoir, forming a secondary oil reservoir, which was the initial stage of oil charging in the Jurassic reservoir. The data from Well MS1 demonstrate that the Tmax and C_{29} sterane 20S/(S + R) thermal evolution parameters in deep and shallow formations are essentially unchanged (Figure 18). The crude oil maturity of both deep and shallow strata is similar, leading to speculation that thermal fluids are flowing from the deep to the shallow reservoirs. This, in turn, provides further evidence that the initial stage of crude oil in the Jurassic period originated from deep reservoirs.
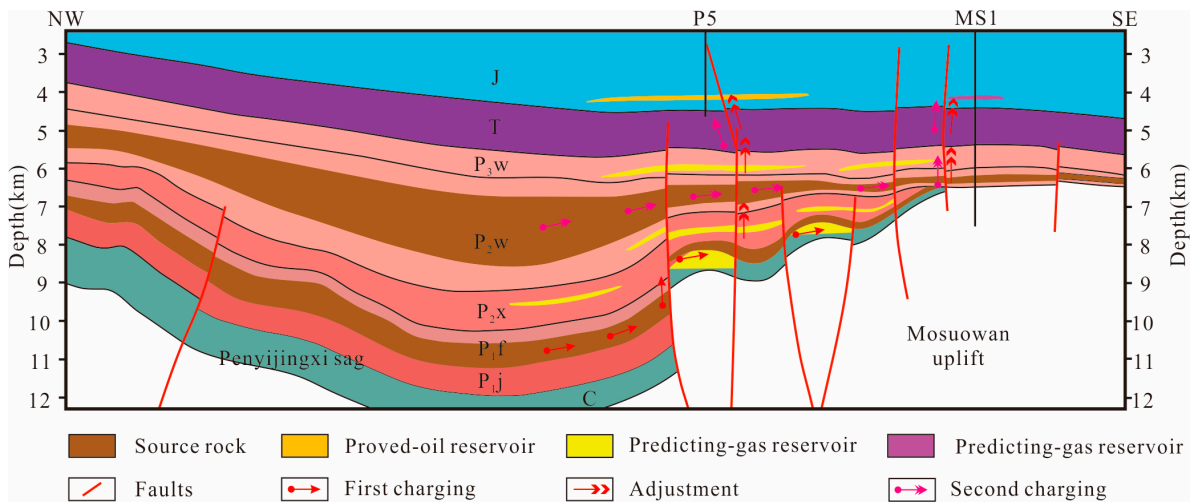
Figure 17. Hydrocarbon accumulation processes in the eastern belt around the Penyijingxi sag.
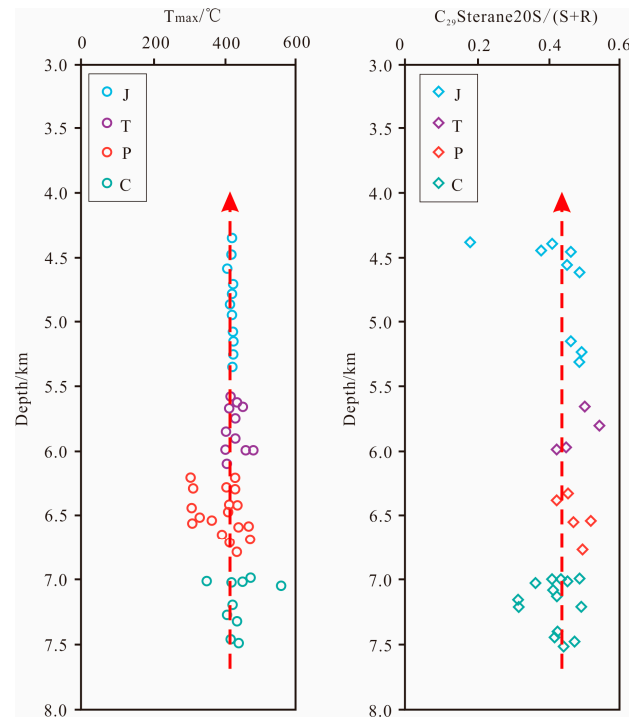

Figure 18. Variation diagram of Tmax and C_{29} sterane 20S/(S + R) of Well Moshen 1 with depth. Notes: J means Jurassic, T means Triassic, P means Permian, C means Carboniferous.

During the Paleogene, the P_1f source rock reached the final stage of hydrocarbon generation, while the P_2w source rock entered a high maturity evolution stage, starting to generate oil and gas. The generated oil and gas were charged into the reservoir of the Jurassic Sangonghe Formation, forming predominantly light oil and gas reservoirs (Figure 17).

5. Conclusions

In the Penyijingxi sag, there exist two sets of source rocks: P_1f and P_2w. The P_1f source rock is a mixed type, consisting of terrigenous plant and aquatic organisms. It belongs to the I-II_1 kerogen, which indicates a high potential for hydrocarbon generation. On the other hand, the P_2w source rock has a higher input of terrigenous plant material, mainly characterized by type III kerogen, making it more prone to gas generation.

The Permian crude oil's parent material was formed in a reducing sedimentary environment, primarily derived from terrigenous plants and aquatic organisms. It exhibits low Pr/Ph ratios, high Gam/C_{30}H values, and a light carbon isotope composition. The tricyclic terpane peak type displays a weak rise and is mainly derived from the P_1f and P_2w source rocks, indicating a mixed-oil characteristic. In contrast, the parent material of Jurassic crude oil was formed in a sedimentary environment, which ranges from weak oxidation to weak reduction. The organic matter is primarily sourced from terrigenous plants. This crude oil possesses high Pr/Ph ratios, low Gam/C_{30}H values, and a heavy carbon isotope composition. The tricyclic terpane peak type is mountain peak, derived predominantly from the P_2w source rock. Regarding Permian natural gas, it exhibits a lighter ethane carbon isotope signature and lower MCC_6 content. It is mainly classified as oil-type gas derived from the P_1f source rock. On the other hand, Jurassic natural gas displays a heavier ethane carbon isotope composition and higher MCC_6 content, indicating a mixed gas primarily composed of coal-type gas.

There are two stages of hydrocarbon accumulation in the Permian reservoir. The first stage charging is the early Jurassic, which matches the oil generation peak period of the P_1f source rock. A large number of blue fluorescent oil inclusions had formed in this stage. At the end of the Cretaceous, the P_1f source rock entered a stage of large amount of gas generation, while the P_2w source rock experienced a peak in oil generation. The generated oil and gas were then charged to the Permian reservoir, undergoing the second stage of charging in the Permian reservoir. Similarly, the Jurassic reservoir also experienced two stages of hydrocarbon charging. The first stage occurred during the early Cretaceous, involving the secondary reservoir formed by crude oil adjustment from the Jurassic underlying reservoirs. From the late Paleogene to the early Neogene periods, the P_2w source rock entered a highly mature stage, generating a large amount of oil and natural gas, which charged into the Jurassic reservoir. This represents the second stage of charging in the Jurassic reservoir, resulting in the present hydrocarbon accumulation primarily composed of light oil and natural gas.

Author Contributions: Methodology, J.Q. and M.H.; Software, Q.Z.; Validation, M.H.; Investigation, Q.Z.; Resources, I.A.; Writing—Original draft, Q.Z.; Writing—Review and editing, J.Q.; Supervision, J.Q. and X.D.; Project administration, X.D.; Funding acquisition, I.A. All authors have read and agreed to the published version of the manuscript.

Data Availability Statement: Restrictions apply to the availability of these data. With permission from PetroChina Xinjiang Oilfield, they can be obtained from the authors.

Conflicts of Interest: The authors declare no conflict of interest.

References

1. Peters, K.E.; Ramos, L.S.; Zumberge, J.E.; Valin, Z.C.; Bird, K.J. De-convoluting mixed crude oil in Prudhoe Bay field, NorthSlope, Alaska. *J. Org. Geochem.* **2008**, *39*, 623–645. [CrossRef]
2. Alizadeh, B.; Alipour, M.; Chehrazi, A.; Mirzaie, S. Chemometric classification and geochemistry of oils in the Iranian sector of the southern Persian Gulf Basin. *Org. Geochem.* **2017**, *111*, 67–81. [CrossRef]
3. Zhan, Z.W.; Tian, Y.; Zou, Y.R.; Liao, Z.; Peng, P. De-convoluting crude oil mixtures from Palaeozoic reservoirs in the Tabei Uplift, Tarim Basin, China. *Org. Geochem.* **2016**, *97*, 78–94. [CrossRef]
4. Zhan, Z.W.; Zou, Y.R.; Pan, C.; Sun, J.N.; Lin, X.H.; Peng, P. Origin, charging, and mixing of crude oils in the Tahe oilfield, Tarim Basin, China. *Org. Geochem.* **2017**, *108*, 18–29. [CrossRef]
5. Carroll, A.R.; Liang, Y.H.; Graham, S.A.; Xiao, X.X.; Hendrix, M.S.; Chu, J.C.; McKnight, C.L. Junggar basin, northwest China: Trapped Late Paleozoic ocean. *Tectonophysics* **1990**, *181*, 1–14. [CrossRef]
6. Hou, M.G.; Zha, M.; Ding, X.J.; Yin, H.; Bian, B.L.; Liu, H.L.; Jiang, Z.F. Source and accumulation process of Jurassic biodegraded oil in the Eastern Junggar Basin, NW China. *Petrol Sci.* **2021**, *18*, 1033–1046. [CrossRef]

7. Zhang, J.; Sun, L.; He, D.X. Biomarker compounds in the source rocks of Upperpedrmian Linxi formation in western Binbei area, Songliao Basin: Characteristics and Implications. *J. Geol. Res.* **2019**, *28*, 350–357. [CrossRef]

8. Koopmans, M.P.; Larter, S.R.; Zhang, C.; Mei, B.; Wu, T.; Chen, Y. Biodegradation and mixing of crude oils in Eocene Es3 reservoirs of the Liaohe basin, northeastern China. *AAPG Bull.* **2002**, *86*, 1833–1843.

9. Lu, X.X.; Jin, Z.J.; Liu, L.F.; Xu, S.L.; Zhou, X.Y.; Pi, X.J.; Yang, H.J. Oil and gas accumulations in the Ordovician carbonates in the Tazhong Uplift of Tarim Basin, west China. *J. Pet. Sci. Eng.* **2004**, *41*, 109–121. [CrossRef]

10. Hao, F.; Zhang, Z.C.; Zou, H.Y.; Zhang, Y.C.; Yang, Y.Y. Origin and mechanism of the formation of the low-oil-saturation Moxizhuang field, Junggar Basin, China: Implication for petroleum exploration in basins having complex histories. *AAPG Bull.* **2011**, *95*, 983–1008. [CrossRef]

11. Zhang, S.C.; Huang, H.P.; Su, J.; Zhu, G.Y.; Wang, X.M.; Larter, S. Geochemistry of Paleozoic marine oils from the Tarim Basin, NW China. Part 4: Paleobiodegradation and oil charge mixing. *Org. Geochem.* **2014**, *67*, 41–57. [CrossRef]

12. Zhu, G.Y.; Su, J.; Yang, H.J.; Wang, Y.; Fei, A.G.; Liu, K.Y.; Zhu, Y.F.; Hu, J.F.; Zhang, B.S. Formation mechanisms of secondary hydrocarbon pools in the Triassic reservoirs in the northern Tarim Basin. *Mar. Pet. Geol.* **2013**, *46*, 51–66. [CrossRef]

13. Moldowan, J.M.; Seifert, W.K.; Gallegos, E.J. Relationship between petroleum composition and depositional environment of petroleum source rocks. *AAPG Bull.* **1985**, *69*, 1255–1268.

14. Nady, M.M.E.; Hussein, S.A.; Ghanem, M.F.; Sharaf, L.M. Oil-source rock correlations of Jurassic and Cretaceous oils in the West Khalda area, North Western Desert, Egypt. *Energy Sources Part A Recovery Util. Environ. Eff.* **2016**, *38*, 330–338. [CrossRef]

15. Deines, P. The carbon isotopic composition of diamonds: Relationship to diamond shape, color, occurrence and vapor composition. *Geochim. Cosmochim. Acta* **1980**, *44*, 943–961. [CrossRef]

16. Stahl, W.J. Source rock-crude oil correlation by isotopic type-curves. *Geochim. Cosmochim. Acta* **1978**, *42*, 1573–1577. [CrossRef]

17. Cao, J.; Wang, X.L.; Sun, P.A.; Zhang, Y.Q.; Tang, Y.; Xiang, B.L.; Lan, W.F.; Wu, M. Geochemistry and origins of natural gases in the central Junggar Basin, northwest China. *Org. Geochem.* **2012**, *53*, 166–176. [CrossRef]

18. Kuang, L.C.; Lv, H.T.; Qi, X.F.; Tang, Y.; Zhang, X. Exploration and targets for lithological reservoirs in Junggar Basin, NW China. *Pet. Explor. Dev.* **2005**, *32*, 32–37.

19. Shi, X.P.; Wang, X.L.; Cao, J.; Hu, W.X.; Yao, S.P.; Xiang, B.L.; Lan, W.F.; Fan, T.L. Genetic type of oils and their migration/accumulation in the Mobei-Mosuowan area, Central Junggar basin. *Acta Sedimentol. Sin.* **2010**, *28*, 380–387.

20. Wang, X.L. Hydrocarbon Source and Accumulation in the Penyijingxi Depression Petroleum System, Central Junggar Basin, NW China. Ph.D. Thesis, Southwest Petroleum Institute, Chengdu, China, 2001.

21. Xiao, Q.L.; He, S.; Yang, Z.; He, Z.L.; Wang, F.R.; Li, S.F.; Tang, D.Q. Petroleum secondary migration and accumulation in the central Junggar Basin, northwest China: Insights from basin modeling. *AAPG Bull.* **2010**, *94*, 937–955. [CrossRef]

22. Conliffe, E.B.; Wilton, D. The use of Integrated fluid inclusion studies for constraining petroleum charge history at Parsons Pond, Western Newfoundland. *Can. Miner.* **2017**, *7*, 39–58. [CrossRef]

23. Lu, Z.Y.; Chen, H.H.; Qing, H.R. Petrography, fluid inclusion and isotope studies in Ordovician carbonate reservoirs in the Shunnan area, Tarim basin, NE China: Implications for the nature and timing of silicification. *Sed. Geol.* **2017**, *359*, 29–43. [CrossRef]

24. Ping, H.W.; Chen, H.H.; Jia, G.H. Petroleum accumulation in the deeply buried reservoirs in the Northern Dongying Depression, Bohai Bay Basin, China: New insights from fluid inclusions natural gas geochemistry and 1-D basin modeling. *Mar. Pet. Geol.* **2017**, *80*, 70–93. [CrossRef]

25. Volk, H.; George, S.C. Using petroleum inclusions to trace petroleum systems a review. *Org Geochem.* **2019**, *129*, 99–123. [CrossRef]

26. Jayanthi, J.L.; Nandakumar, V. Fluid Inclusion studies to determine the palaeotemperature and hydrocarbon quality of oils in petroliferous basins. *J. Petrol. Sci. Eng.* **2021**, *197*, 108082. [CrossRef]

27. Wang, G.R. Classification of tectonic units and geologic evolution in the northern Xinjiang and neighboring area. *Xinjiang Geol.* **1996**, *14*, 12–27.

28. Li, J.Y.; He, G.Q.; Xu, X.; Li, H.Q.; Sun, G.H.; Yang, T.N.; Gao, L.M.; Zhu, Z.X. Crustal tectonic framework of Northern Xinjiang and adjacent regions and its formation. *Acta Sedimentol. Sin.* **2006**, *80*, 148–168.

29. Zhao, J.M.; Ma, Z.J.; Yao, C.L. Analysis on gravity-magnetic anomalies in basement geotectonic divisions in the Junggar Basin. *Xinjiang Pet. Geol.* **2008**, *29*, 7–11.

30. Liu, K.S.; Qu, J.X.; Zha, M.; Liu, H.L.; Ding, X.J.; Zhou, M.H.; Gao, T.Z. Genesis Types and Migration of Middle and Lower Assemblages of Natural Gas in the Eastern Belt around the Penyijingxi Sag of the Junggar Basin, NW China. *Processes* **2023**, *11*, 689. [CrossRef]

31. Windley, B.F.; Alexeiev, D.; Xiao, W.; Kröner, A.; Badarch, G. Tectonic models for accretion of the Central Asian Orogenic Belt. *J. Geol. Soc.* **2007**, *164*, 31–47. [CrossRef]

32. Ding, X.J.; Gao, C.H.; Zha, M.; Chen, H.; Su, Y. Depositional environment and factors controlling β-carotane accumulation: A case study from the Jimsar Sag, Junggar Basin, northwestern China. *Palaeogeogr. Palaeoclimatol. Palaeoecol.* **2017**, *485*, 833–842. [CrossRef]

33. Cao, J.; Zhang, Y.; Hu, W.; Yao, S.; Wang, X.; Zhang, Y.; Tang, Y. The Permian hybrid petroleum system in the northwest margin of the Junggar Basin, NW China. *Mar. Pet. Geol.* **2005**, *22*, 331–349. [CrossRef]

34. Zhou, W.Q.; Luo, X.L.; Liu, H.W. Analysis of hydrocarbon reservoir forming in the east belt around Pengyijingxi depression. *Xinjiang Oil Gas.* **2005**, *1*, 16–20.

35. Golyshev, S.I.; Verkhovskaya, N.A.; Burkova, V.N.; Matis, E.Y. Stable carbon isotopes in source-bed organic matter of West and East Siberia. *Org. Geochem.* **1991**, *17*, 277–291. [CrossRef]

36. Tissot, B.P.; Wilt, D.H. *Petroleum Formation and Distribution*; Petrol. Ind. Press: Beijing, China, 1982.

37. Wang, X.L.; Zhi, D.M.; Wang, Y.T.; Chen, J.P.; Qin, Z.J.; Liu, D.G.; Xiang, Y.; Lan, W.F.; Li, N. *Source Rocks and Oil-Gas Geochemistry in Junggar Basin*; Petrol. Ind. Press: Beijing, China, 2013.

38. Shanmugam, G. Significance of coniferous rain forests and related organic matter in generating commercial quantities of oil, Gippsland Basin, Australia. *AAPG Bull.* **1985**, *69*, 1241–1254. [CrossRef]

39. Peters, K.E.; Snedden, J.W.; Sulaeman, A.; Sarg, J.F.; Enrico, R.J. A New Geochemical-Sequence Stratigraphic Model for the Mahakam Delta and Makassar Slope, Kalimantan, Indonesia. *AAPG Bull.* **2001**, *85*, 1102–1105.

40. Peng, X.F.; Li, Z.B. The application of biomarker in the research of petroleum geology. *Res. Env. Eng.* **2006**, *20*, 279–283.

41. Didyk, B.M.; Simoneit, B.R.T.; Brasselll, S.C.; Eglinton, G. Organic geochemical indicators of palaeoenvironmental conditions of sedimentation. *Nature* **1978**, *272*, 216–222. [CrossRef]

42. Hughes, W.B.; Holba, A.G.; Dzou, L.I.P. The ratios of dibenzothiophene to phenanthrene and pristane to phytane as indicators of depositional environment and lithology of petroleum source rocks. *Geochim. Cosmochim. Acta.* **1995**, *59*, 3581–3598. [CrossRef]

43. Wang, X.L.; Kang, S.F. The oil source of the Mabei oil field, northwest Junggar Basin. *J. SW. Pet. Inst.* **2001**, *23*, 6–8.

44. Peters, K.E.; Walters, C.C.; Moldowan, J.M. *The Biomarker Guide: Biomarkers and Isotopes in Petroleum Systems and Earth History*, 2nd ed.; Cambridge University Press: Cambridge, UK, 2005; p. 1155.

45. Jiang, Z.S.; Fowler, M.G. Carotenoid-derived alkanes in oils from northwestern China. *Org. Geochem.* **1986**, *10*, 831–839. [CrossRef]

46. Grande, S.M.B.; Aqunio, N.F.R.; Mello, M.R. Extended tricyclic terpanes in sediments and petroleums. *Org. Geochem.* **1993**, *20*, 1039–1047. [CrossRef]

47. Philp, P.; Symcox, C.; Wood, M.; Nguyen, T.; Wang, H.; Kim, D. Possible explanations for the predominance of tricyclic terpanes over pentacyclic Sterpanes in oils and rock extracts. *Org. Geochem.* **2021**, *155*, 104220. [CrossRef]

48. Xiao, H.; LI, M.; Yang, Z.; Zhu, Z. Distribution patterns and geochemical implications of C_{19}-C_{23} tricyclic terpanes in source rocks and crude oils occurring in various depositional environments. *Geochimica* **2019**, *48*, 161–170. [CrossRef]

49. Aichner, B.; Herzschuh, U.; Wilkes, H. Influence of aquatic macrophytes on the stable carbon isotopic signatures of sedimentary organic matter in lakes on the Tibetan Plateau. *Org. Geochem.* **2010**, *41*, 706–718. [CrossRef]

50. Xia, L.; Cao, J.; Lee, C.; Stüeken, E.E.; Zhi, D.; Love, G.D. A new constraint on the antiquity of ancient haloalkaliphilic green algae that flourished in a ca. 300 Ma Paleozoic lake. *Geobiology* **2021**, *19*, 147–161. [CrossRef]

51. Hou, M.G.; Qu, J.X.; Zha, M.; Swennen, R.; Ding, X.J.; Ablimiti, Y.M.; Liu, H.L.; Bian, B.L. Significant contribution of haloalka-liphilic cyanobacteria to organic matter in an ancient alkaline lacustrine source rock: A case study from the Permian Fengcheng Formation, Junggar Basin, China. *Mar. Petrol. Geol.* **2022**, *138*, 105546. [CrossRef]

52. Jamesa, T. Correlationofnaturalgasbyuseof carbon isotopic distribution between hydrocabon components. *AAPG Bull.* **1983**, *74*, 1176–1191.

53. Dai, J.X. Significance of the study on carbon isotopes of alkane gases. *Nat. Gas Ind.* **2011**, *31*, 1–6.

54. Alexei, V.M.; Mohinudeen, F.; Giuseppe, E. Geochemistry of shale gases from around the world: Composition, origins, isotope reversals and rollovers, and implications for the exploration of shale plays. *Org. Geochem.* **2020**, *143*, 103997. [CrossRef]

55. Liu, Q.; Wu, X.; Wang, X.; Jin, Z.; Zhu, D.; Meng, Q.; Fu, Q. Carbon and hydrogen isotopes of methane, ethane, and propane: A review of genetic identification of natural gas. *Earth-Sci. Rev.* **2019**, *190*, 247–272. [CrossRef]

56. Mango, F.D. The light hydrocarbons in petroleum: A critical review. *Org. Geochem.* **1997**, *26*, 417–440. [CrossRef]

57. Hu, T.L.; Ge, B.X.; Zhang, Y.G.; Liu, B. Development and application of fingerprint parameters of source rock adsorbed hydrocarbon and natural gas light hydrocarbon. *Pet. Geol. Exp.* **1990**, *12*, 375–394, 450.

58. Leythaeuser, D.; Schaefer, R.; Cornford, C.; Weiner, B. Generation and migration of light hydrocarbons (C_2–C_7) in sedimentary basins. *Org. Geochem.* **1979**, *1*, 191–204. [CrossRef]

59. Munz, I.A. Petroleum inclusions in sedimentary basins: Systematics, analytical methods and applications. *Lithos* **2001**, *55*, 195–212. [CrossRef]

60. Zhao, Y.J.; Chen, H.H. The relationship between fluorescence colors of oil inclusions and their maturities. *J. Earth Sci. J. China Univ. Geos.* **2008**, *33*, 91–96. [CrossRef]

61. Bodnar, R. Petroleum migration in the Miocene Monterey Formation, California, USA: Conception, classification, formation mechanism and significance. *Eur. J. Miner.* **2006**, *25*, 19–26.

62. Eadington, P.J.; Hamilton, P.J.; Bai, G.P. Fluid history analysis—A new concept for prospect evaluation. *APEA J.* **1991**, *31*, 282–294. [CrossRef]

63. Lin, H.M.; Cheng, F.Q.; Wang, Y.S. Fluid inclusion evidence for multiperiod oil charge in Shahejie member 4, Bonan subsag, Bohai Bay Basin. *Oil Gas Geol.* **2017**, *38*, 209–218. [CrossRef]

64. Si, S.H.; Chen, H.H.; Feng, Y.; Wang, Y. Two sources and three charging events of hydrocarbons in Lower Cretaceous reservoirs in Shaya uplift, Tarim Basin: Evidence from fluid inclusion analysis. *Acta Pet. Sin.* **2013**, *34*, 12–21. [CrossRef]

65. Goldstein, R.H. Fluid inclusions in sedimentary and diagenetic systems. *Lithos* **2001**, *55*, 159–193. [CrossRef]

66. Li, J.; Zha, M. Determination of oil accumulation period and building up of paleopressure of Wumishan formation in Renqiu Oilfield by using fluid inclusion. *J. China Univ. Petrol. (Ed. Nat. Sci.)* **2010**, *34*, 38–43. [CrossRef]

67.   Middleton, D.; Parnell, J.; Carry, P.; Xu, G. Reconstruction of fiuld migration history in northwest Ireland using fluid inclusion studies. *J. Geochem Explor.* **2000**, *69–70*, 673–677. [CrossRef]

68.   Volk, H.; George, S.C.; Middleton, H.; Schofield, S. Geochemical comparison of fluid inclusion and present-day oil accumulations in the Papuan Foreland—Evidence for previously unrecognised petroleum source rocks. *Org. Geochem.* **2005**, *36*, 29–51. [CrossRef]

69.   Liu, L.J.; Richards, J.P.; DuFrane, S.A.; Rebagliati, M. Geochemistry, geochronology, and fluid inclusion study of the Late Cretaceous Newton epithermal gold deposit, British Columbia. *Can. J. Earth Sci.* **2016**, *53*, 10–33. [CrossRef]

70.   Liu, K.; George, S.C.; Lu, X.; Gong, S.; Tian, H.; Gui, L. Innovative fluorescence spectroscopic techniques for rapidly characterising oil inclusions. *Org. Geochem.* **2014**, *72*, 34–45. [CrossRef]

71.   Liu, K.Y.; Eadington, P. Quantitative fluorescence techniques for detecting residual oils and reconstructing hydrocarbon charge history. *Org. Geochem.* **2005**, *36*, 1023–1036. [CrossRef]

72.   Ma, W.J.; Wang, R.; Wang, F.; Li, X.L. Application of Quantitative Grain Fluorescence Technique in Restoration of Hydrocarbon Charging History of Jurassic Reservoirs in Mosuowan Swell, Junggar Basin. *Xinjiang Pet. Geol.* **2016**, *37*, 524–529.